
Copyright 2018, ABRACO

Trabalho apresentado durante o INTERCORR 2018, em São Paulo, no mês de maio de 2018.

As informações e opiniões contidas neste trabalho são de exclusiva responsabilidade do(s) autor(es).

Microstructural and Electrochemical behavior of Welded Pipe A106 Gr. B and 316L with nickel alloys 82 and 182 in 3.5 wt. % NaCl solution

Alisson H. Freire Vilela¹, Wagner R. Costa Campos², Luiza Esteves³, Camila R. Oliveira Almeida⁴, Bárbara A. Cardoso⁵, Emerson G. Rabelo⁶

Abstract

The aim of this work was to investigate the microstructure and evaluate the corrosion behavior of dissimilar metal welded between carbon steel pipe A106 Gr B and 316L austenitic stainless steel with nickel alloy 82 and 182 as filler metals. These welded joints were analyzed in three different conditions, as welded (AW), after post weld heat treatment (PWHT) and after weld overlay (WOL), both used to minimize the residual stress effect. Electrochemical tests were carried out considering three types of samples: weld joint, A106 B and 316L steel base metal in 3.5% NaCl solution. Tafel extrapolation was used to calculate the corrosion rate. For weld joint, welding heat cycle changed the microstructure of the heat affect zone (HAZ) on root weld causing an intense grain refinement and polygonal ferrite and perlite formation. Otherwise, on finish weld was observed allotriomorphic ferrite, polygonal ferrite, acicular ferrite, ferrite with martensite/austenite/carbides aligned and pearlite to AW and PWHT conditions. Polygonal ferrite and perlite were observed in WOL condition. Similar corrosion rates among the three conditions of each sample were observed. Base metal 316L showed the lowest corrosion rate following by welded joint and finally base metal A106 B.

Keywords: A106 Gr B carbon steel; 316L stainless steel; corrosion; dissimilar metal weld; Tafel extrapolation

Introduction

Dissimilar metal weld (DMW) involving austenitic stainless steel and ferritic carbon steels are applied in petrochemical, thermoelectrical, nuclear, coil industries and distinct engineering structures as heat exchangers, nozzles, boilers, pressure vessels and so on (1–3). The auxiliary use of carbon steels in strategic locals pipe system gives reduction costs, since are cheaper related to austenitic stainless steels and gives better mechanical properties weld due to joining metals employed (4-6).

The weld process creates a residual stress due to different physical and mechanical properties at structure steels (2). Therefore, nickel alloys are employed by having intermediate values,

¹Mestrando; Engenheiro Químico - Centro de Desenvolvimento de Tecnologia Nuclear

²Pesquisador; Engenheiro Mecânico - Centro de Desenvolvimento de Tecnologia Nuclear

³Pós Doutoranda; Química - Centro de Desenvolvimento de Tecnologia Nuclear

⁴Estudante; Engenheira Metalúrgica - Centro de Desenvolvimento de Tecnologia Nuclear

⁵Estudante; Engenheira Química - Centro de Desenvolvimento de Tecnologia Nuclear

⁶Pesquisador; Engenheiro Metalúrgico - Centro de Desenvolvimento de Tecnologia Nuclear

which decreases this difference between ferritic carbon and austenitic stainless steels, and good resistance to corrosion and failure (7-10).

Stress corrosion cracking (SCC) may come from residual stress and leads to crack formation at metallurgical susceptible metal due to simultaneous action of present residual stress and corrosion environment. Continuous interaction with seawater, mainly chloride particles, threats pipe system physical integrity through corrosion effects imposed to its structure. This type corrosion is very present at oil extraction environment and nuclear power plants, for instance (11-14).

In order to reduce SCC susceptibility, related to residual stress effects, a post weld heat treatment (PWHT) may be applied to relief stress at welded joints (15-16). At crack presence, a weld overlay (WOL) may be applied to impose a compressive tension (opposite to stress tension caused by residual stress) and a mechanical and corrosive barrier to crack propagation (7).

Due to importance application of this weld type, this work aims analyze the corrosion effects in marine environment, with NaCl 3.5% wt. solution, at base metals and welded joints after PWHT and WOL. Their corrosion rate was obtained through Tafel extrapolation e compared to welded joint as welded (AW). In addition, the microstructure of these base metals and joints were characterized by optical microscopy (OM).

Methodology

Materials and Methods

DMW pipe joints were composed of a seamless carbon steel pipe (ASTM A-106 Gr. B) and a seamless austenitic stainless steel pipe (ASTM A-312 TP316L), schedule 160 with diameter of 168.2 mm and wall thickness of 18.3 mm, with length of 150 mm, and two different filler metals, the nickel alloy 82 (AWS A5.14 ER NiCr-3) with 2.0 mm diameter, buttering and root layers weld, by gas tungsten arc welding (GTAW), and nickel alloy 182 (AWS A5.11 E NiCrFe-3) with diameter of 3.25 mm to fill welding, shielded metal arc welding (SMAW). The chemical compositions of the base metals and weld metals are summarized in Table 1. asdasdasdasdasdasdasdasdasdasdasdasdasdasdas

Welding, post weld heat treatment and weld overlay

The pipes were machined, bevelled at 30° V format and 200 °C preheated. Root weld about 2.00 mm was composed by two welding beads and buttering layer about 5.00 mm thickness composed by three welding beads, both nickel alloy 82 by GTAW process. Seven layers of nickel alloy 182 coated electrode was applicated as filler weld metal by SMAW process. Root, buttering and fill interpasses were applied at range temperature of 140 °C to 170 °C. The welding main parameters and the final DMW may be seen in Table 2 and Figure 1, respectively.

A thermal blanket was positioned at center weld, with width about 100.00 mm to each side, and heated the welded joint at 620 °C during 2.5 h, with 220 °C/h heating rate. Cooling was done with thermal blanket turned off between 620 °C and 300 °C with cooling rate about 400 °C/h and between 300 °C and 100 °C with cooling rate about 75 °C/h. PWHT steps to stress

relief must include a moderated heating rate, residence time at range temperature between 600 °C and 700 °C to ferritic carbon steels and about 900 °C to austenitic stainless steel and cooling low rate to avoid new residual stress (15,17-19).

The weld overlay was applied at weld center with five layers of nickel alloy 82 by GTAW process, with 115.00 mm length, about 45.0 mm to each side, and 7.00 mm thickness, according to Figure 2:

Both PWHT and WOL applied in this study were efficient to reduce internal residual stress of this welded sets through microhardness Vickers and Hole Drilling Strain Gage (22,23).

Metallographic analisys

The samples were extracted from longitudinal section of welded sets and were identified according to dissimilar weld original set: as welded (AW), with PWHT (PWHT) and with weld overlay (WOL). The weld joints samples (WJ) encompass metal base parts, ASTM A-106 Gr. B e ASTM 312 TP316L, their HAZ's and weld metals 82 and 182. Whereas base metals (BM) samples were extracted from side of WJ samples. After, a wire was solded at each sample before cold mounting in resin epoxy. The working surface to WJ samples was 7.00 cm² and 3.00 cm² to BM samples. Then, the samples were cold mounted in resin epoxy, grinded in 80#, 220#, 400#, 600#, 1200# e 2000# SiC paper, polished with diamond paste 6 µm, 3 µm and 1 µm, rinsed with distilled water and ethyl alcohol and dried with hot air before metallographic analisys.

Macrostructure was revealed by exposing samples to Nital's reagent 2% (2.0mL nitric acid and 98.0 mL ethyl alcohol) during 10 s by imersion, followed by Marble's reagent exposition (4.0 g CuSO₄, 20.0 mL HCl and 20.0 mL distilled water) during 120 s by imersion, and over again, with cotton smearing, by Marble's reagent during 15 s. Microstructure was revealed by exposing samples to Nital's reagent 2% during 10 s and electrolytic etching with oxalic acid solution 10% wt. (10.0 g and 100.0 mL distilled water), 2.0 V during 120 s. Metallographic examination was carried out using Leica DM4500P optical microscopy.

Electrochemical tests

After metallographic examination, the samples were grinded again in 80#, 220#, 400#, 600#, 1200# SiC paper, rinsed with distilled water and ethyl alcohol and dried with hot air before electrochemical tests.

Potentiodynamic polaratization tests were carried out at least five times to acquire reproducibility at room temperature. An electrochemical cell with silver/silver chloride (Ag/AgCl, 3M KCl) as reference electrode platinum as counter electrode and samples as working electrodes was used with NaCl 3.5% wt. (g/L) solution. The open circuit potential (OCP) was monitored and measured after 900 s (15 min) until its stabilization. Afterward, a scan rate of 0.5 mV/s was applied, starting at - 250.0 mV (Ag/AgCl) to + 250.0 mV (Ag/AgCl), related to OCP. A potentiostat Autolab PGSTAT 100 were employed and polarization curves were produced by software *NOVA 2.0*. Corrosion rates (i_{corr}) were obtained through Tafel extrapolation with auxiliar equations 1 and 2 (21-22):

$$\eta_a = b_a \cdot \log (i_a / i_{\text{corr}}) \quad (1)$$

$$\eta_c = b_c \cdot \log (i_c / i_{\text{corr}}) \quad (2)$$

where, η_a e η_c , as anodic and cathodic polarization; b_a e b_c , as anodic and cathodic Tafel slopes; and i_a e i_c , as anodic and cathodic current densities.

Results and discussion

Metallographic analysis

The surface of the longitudinal section was ground, polished and attacked with Marble and Nital 2% reagents to reveal macrostructure. Figure 3 shows the etched macrostructure of the DMW with carbon steel A-106 Gr. B and stainless steel TP316L pipes, with Alloy 82 (Ni 82) buttering and root weld and Alloy 182 (Ni 182) fill weld metal.

Figure 4 shows microphotographs DMW samples AW (a), PWHT (b) and WOL (c), etched by Nital 10% at 10 seconds plus Marble at 120 seconds plus swab for 15 seconds.

The microstructure of the BM A 106 B samples to all conditions, showed by Figure 5, etching Nital 3% during 10 seconds, consists of the ferrite (dark areas) and perlite (light areas) grains, with 10 μm grain size. According to Figure 6, the microstructure of MB 316L samples etching with oxalic acid 10% with 3V during 120 seconds, consists of equiaxial austenite grains, with 60 μm grain size, to all conditions. Dendrites grains were observed with inclusions and precipitates in WJ sample to all conditions AW (6a), PWHT (6b) and WOL (6c), both nickel alloys 82 root pass and nickel alloys 82 top pass, according to Figure 6

About Figure 7, microstructure observed in ZTA root weld between carbon steel A106 B and nickel alloy 82 to WJ sample showed polygonal ferrite and fine perlite to all conditions (7a, 7b and 7c). On finish weld region to AW and PWHT conditions (7d and 7e) were observed polygonal ferrite (PF), grain boundary allotriomorphic ferrite F(GBA), acicular ferrite (AF), perlite (P) and ferrite with martensite/austenite/carbides aligned F(AC) (28). The weld overlay applied at WOL condition (7f) caused a grain refinement of polygonal structure. HAZ microstructure of austenitic stainless steel 316L with nickel alloy 182 was composed by growth austenitic grains to all conditions without deleterious phases.

According Figure 8, to WJ sample of WOL condition was observed growth austenitic grains in HAZ between weld overlay and austenitic stainless steel 316L (8a). The HAZ between weld overlay and carbon steel A106 B showed grain size refinement with ferrite polygonal equiaxed grains (8b).

Electrochemical tests

The potentiodynamic polarization Tafel scans of welded joint (WJ), base metals ASTM A106 Gr. B (A 106 B) and ASTM 312 TP316L (316L) samples show their electrochemical behavior at 3.5% wt. NaCl solution through Figure 9a, Figure 9b and Figure 9c, respectively. In addition, the parameters of each test are listed in Table 3 to WJ samples, Table 4 to A 106 B samples and Table 5 to 316L samples.

Polarization curves of conditions AW, PWHT and WOL were very similar at each sample. The noblest corrosion potential was appointed by 316L samples, followed by WJ samples and finally, A 106 B samples. Presence of filler metals nickel alloys may be the reason for this intermediate position for WJ since such alloys are more resistant to corrosion (7-10). Both WJ and A1 06 B polarization curves were predominately under anodic control unlike 316L that was more influenced by cathodic reaction (27).

These similar curves behaviors lead to similar corrosion rate among conditions at each sample, according Table 3, Table 4 and Table 5. Even considering standard deviation, this similarity was maintained due to insignificant difference results between them. In addition, the punctual presence of F(GBA), AF, PF, P and F(AC) microstructures at HAZ region between carbon steel A106 B and nickel alloy 82 top pass were not sufficient to cause significantly changes in electrochemical results, however some researches had been reported the influence of the microstructure in the corrosion behavior (2, 24-31).

Conclusions

DMW sets involving carbon steel ASTM A-106 Gr. B, austenitic stainless steel ASTM 312 TP316L with nickel alloy 82 and 182 as filler metals was evaluated about corrosion effects in NaCl 3.5% wt. solution through corrosion rate comparison among AW, PWHT and WOL conditions. Furthermore, their microstructure were acquired

Microstructure of BM A106-B and BM 316L samples revealed no significant variation about all conditions. Related to WJ samples, at 316L HAZ root weld and finish weld was observed growth austenitic grains without deleterious phases to all conditions, whereas at A-106 B HAZ root weld were observed polygonal ferrite and perlite to all conditions, too. Finish weld region at A-106 B HAZ showed presence of polygonal ferrite (PF), grain boundary allotriomorphic ferrite F(GBA), acicular ferrite (AF), perlite (P) and ferrite with martensite/austenite/carbides aligned F(AC) microstructures to AW and PWHT samples. At this region to WOL condition was observed a grain refinement. The HAZ between weld overlay and A-106 B caused grain size refinement of ferrite polygonal equiaxed grains and the HAZ between weld overlay and 316L caused growth austenitic grains. Dendrites grains were observed at nickel alloys 82 and 182.

Electrochemical results showed the smallest corrosion rate to BM 316L, followed by WJ e, finally BM A-106 G samples. It was not possible appoint the best condition (AW, PWHT and WOL) of each sample (WJ, BM A-106 B and BM 316L) due to similar behaviors of showed polarization curves and, consequently, similar results. Although some observed microstructures could be decisive to electrochemical results, as acicular ferrite and polygonal ferrite for instance, their punctual presence was not sufficient for that.

This work continues and its forward step will consist to evaluate susceptibility SCC of these DMW sets in NaCl 3.5% wt. solution at room temperature by slow strain rate test.

Acknowledgments

The authors of this work wish thank the research funding institutes CAPES, CNPQ e FAPEMIG for the financial support and to CNEN e CDTN for installations and support team.

Figures

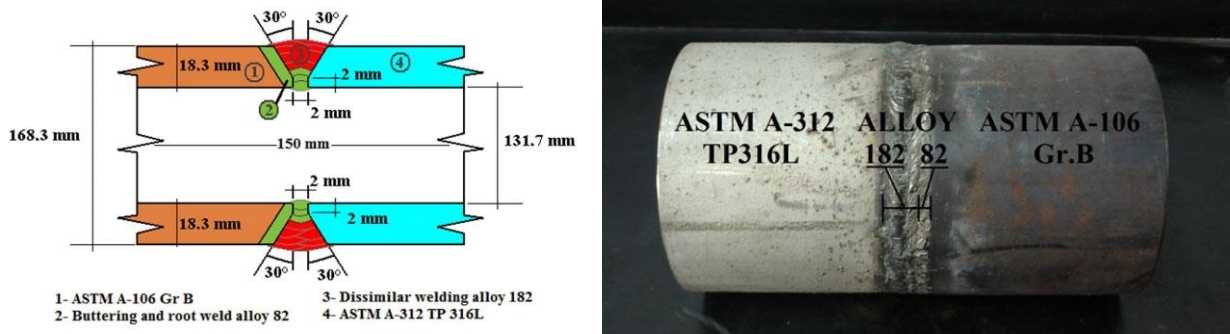


Figure 1 – Schematic representation of DMW pipe (left) and DMW pipe (right)



Figure 2 – Weld overlay applied at welded region dissimilar joint.

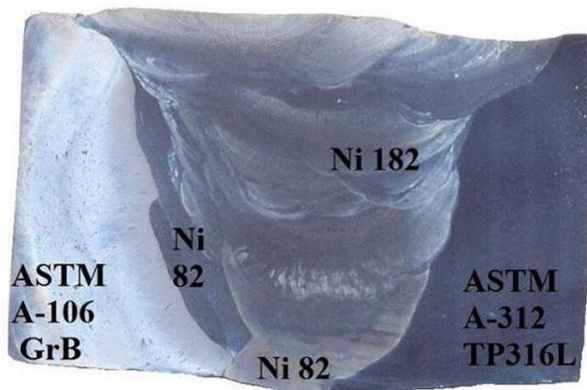


Figure 3 – Longitudinal surface section of DMW after metallographic characterization. Nital 2% and Marble.

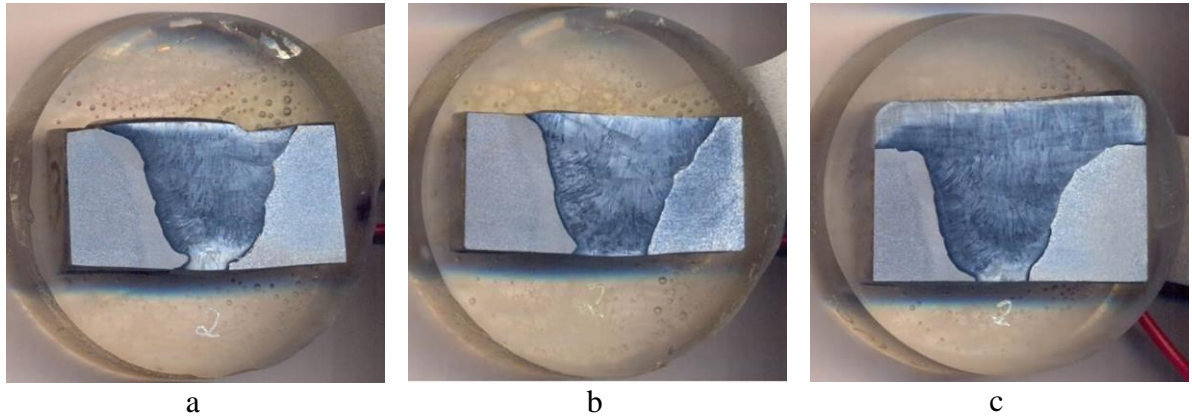


Figure 4 – Longitudinal section of DMW (a) AW, (b) PWHT and (c) WOL. Nital 2% and Marble.

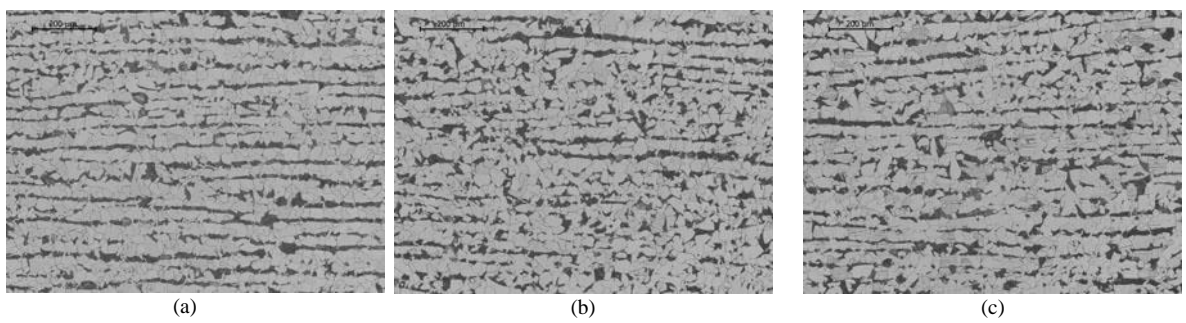


Figure 5 – Micrographics of BM A106 B samples of AW (a), PWHT (b) and WOL (c), conditions.

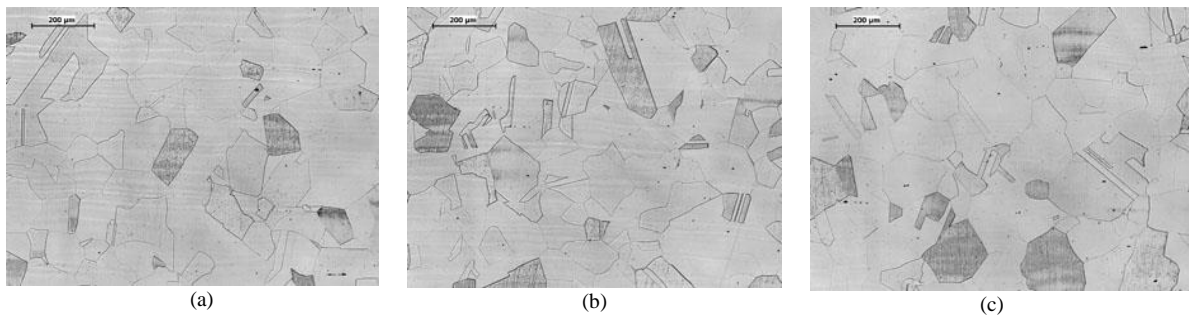
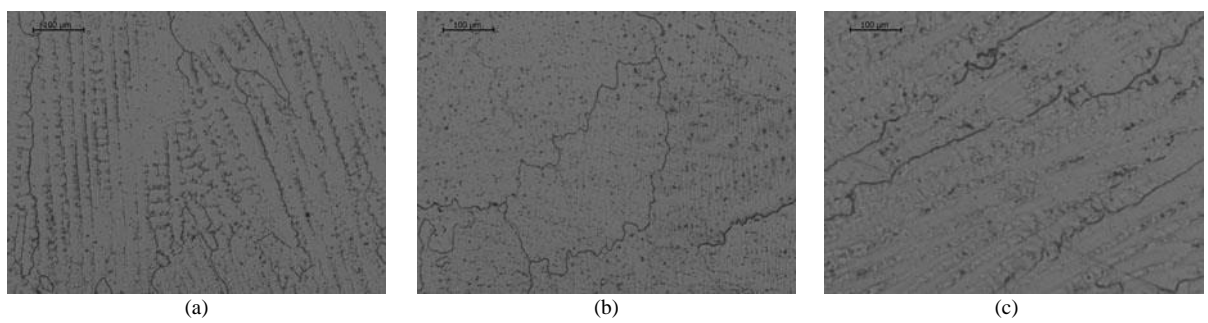


Figure 6 - Micrographics of BM 316L samples to AW (a), PWHT (b) and WOL (c) conditions.



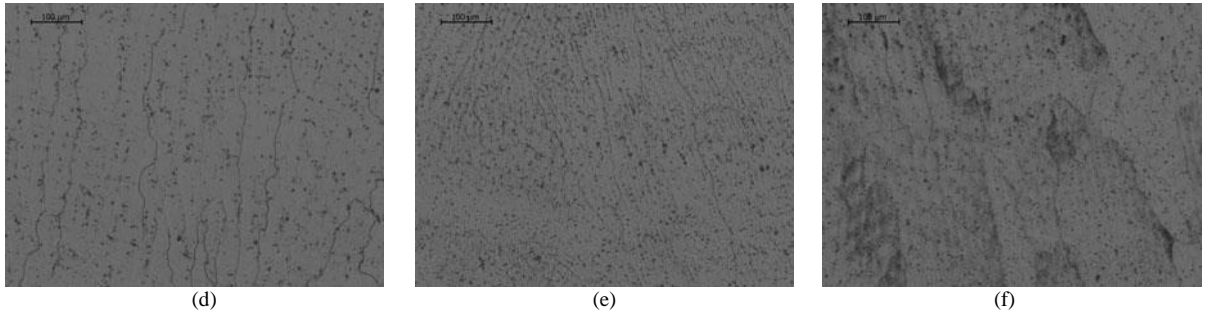


Figure 6 – Micrographics root pass (a, b and c) of nickel alloys 82 and top pass (d, e and f) pass with nickel alloy 182 to AW (a, d), PWHT (b, e) and WOL (c, f) conditions.

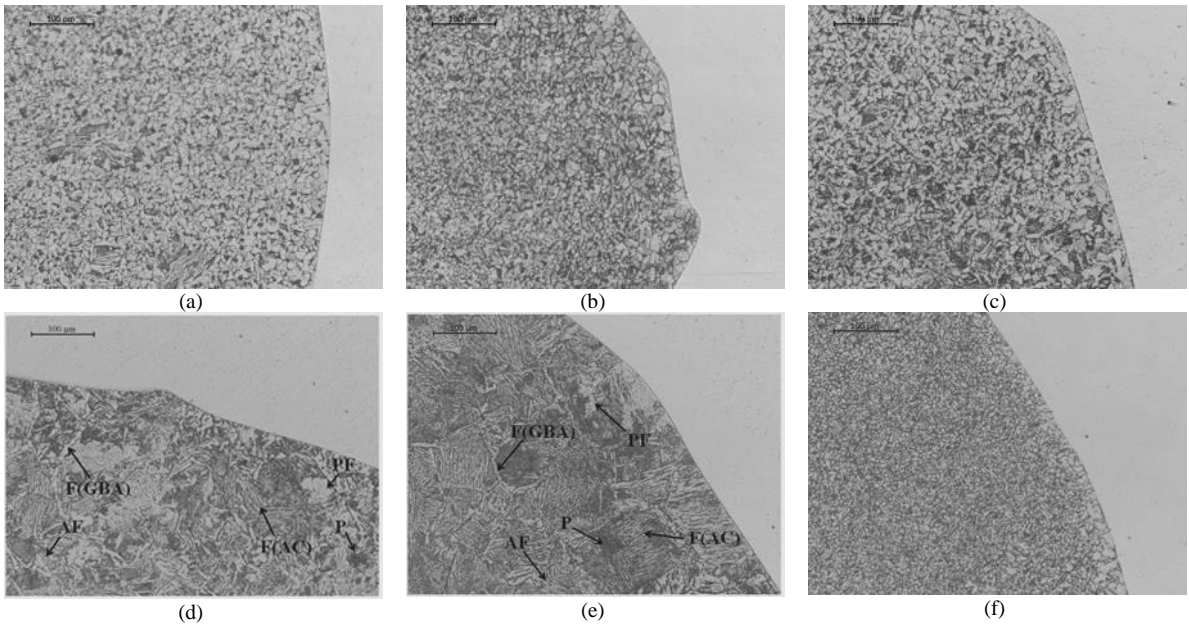


Figure 7 – Micrographics of MB A106 B samples showing ZTA root (a, b and c) and top (d, e and f) pass with nickel alloy 82 to AW (a, d), PWHT (b, e) and WOL (c, f) conditions.

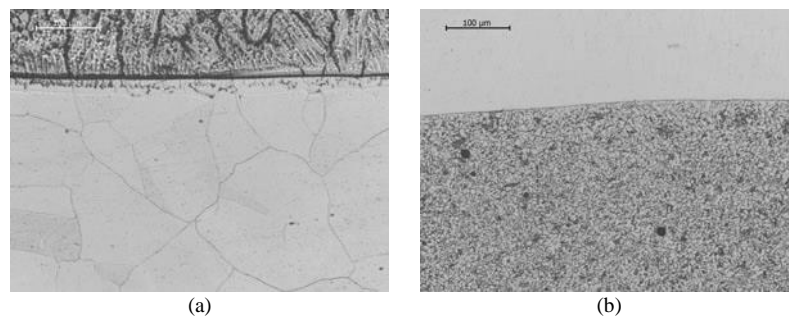
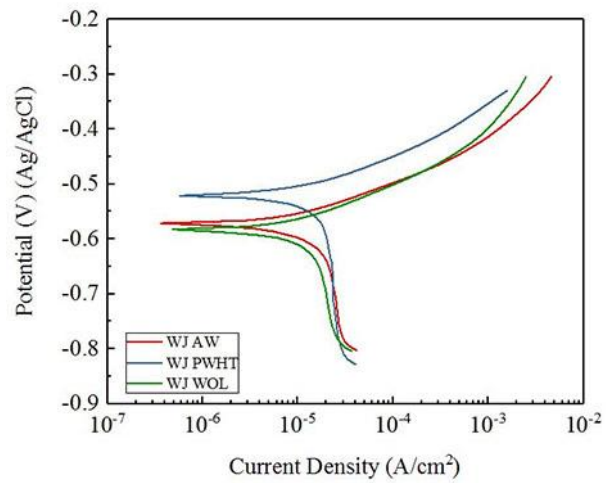
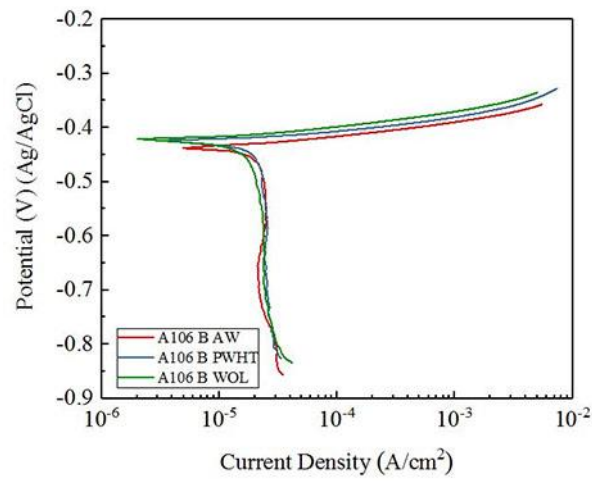


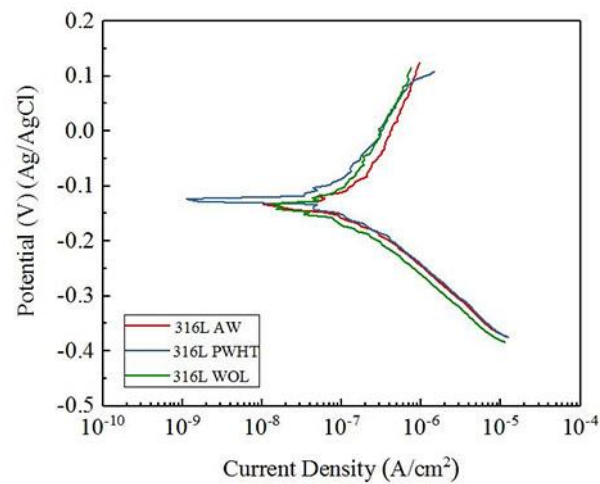
Figure 8 – Micrographics ZTA's regions of 316L (a) and A106 B (b) of WJ sample in WOL condition.



(a)



(b)



(c)

Figure 9 –Polarization Tafel scans of WJ (a), A106 B (b) and 316L (c) samples at each condition.

Tables

Table 1 – Nominal chemical composition (wt. %) of pipes and filler metals.

Metal/Elem.	C	Mn	Si	Cr	Mo	Nb	Ti	Ni	Fe
A-106	0.30	0.29-1.06	0.10	0.40	0.15	-	-	0.40	Bal
316L	0.035	2.00	1.00	16.00-18.00	2.00-3.00	-	-	10.00-14.00	Bal
82	<0.10	2.50-3.50	<0.015	18.00-22.00	-	2.00-3.00	<0.75	>67.00	<3.00
182	<0.10	5,00-9.50	<0.015	13.00-17.00	-	1.00-2.50	<1.00	>59.00	<10.00

Table 2 – Welding parameters of DMW fabrication.

Local/filler metals	Process	Rod (mm)	Current (A)	Voltage (V)	Velocity(mm/s)
Butter/82	GTAW	2.00	120-150	10.0-12.0	2.40-3.20
Root weld/82	GTAW	2.60	110-120	19.0-21.0	0.80-1.20
Fill weld/182	SMAW	3.60	115-130	20.0-22.0	1.50-2.00

Table 3 – Tafel parameters of JS samples at each condition.

Condition	E_{corr} (Ag/AgCl) (V)	i_{corr} (10^{-6} A/cm ²)	Corrosion Rate (mm/year)
AW	-0.589 ± 0.022	2.93 ± 0.77	0.03 ± 0.01
PWHT	-0.517 ± 0.032	4.43 ± 0.74	0.05 ± 0.01
WOL	-0.589 ± 0.018	4.01 ± 0.16	0.05 ± 0.00

Table 4 – Tafel parameters of A106 B samples at each condition.

Condition	E_{corr} (Ag/AgCl) (V)	i_{corr} (10^{-5} A/cm ²)	Corrosion Rate (mm/year)
AW	-0.440 ± 0.010	1.08 ± 0.13	0.13 ± 0.02
PWHT	-0.425 ± 0.007	1.31 ± 0.01	0.15 ± 0.01
WOL	-0.439 ± 0.032	3.78 ± 0.01	0.17 ± 0.00

Table 5 – Tafel parameters of 316L samples at each condition.

Condition	E_{corr} (Ag/AgCl) (V)	i_{corr} (10^{-8} A/cm ²)	Corrosion Rate (μ m/year)
AW	-0.153 ± 0.016	7.23 ± 0.46	0.84 ± 0.05
PWHT	-0.118 ± 0.029	4.33 ± 0.84	0.50 ± 0.10
WOL	-0.139 ± 0.027	5.66 ± 0.63	0.66 ± 0.07

Referências bibliográficas

- (1) ZHU, R. et al. Stress corrosion cracking of 316L HAZ for 316L stainless steel/Inconel 52M dissimilar metal weld joint in simulated primary water. **Corrosion Science**, Beijing, v. 112, p. 373-384, Nov. 2016.
- (2) HUANG, B. S. et al. Study on the microstructure, mechanical properties and corrosion behaviour of S355JR/316L dissimilar welded joint prepared by gas tungsten arc welding multi-pass welding process. **Science Technology of Welding and Joining**, Chengdu, v. 21, n. 5, p. 381-388, Apr. 2016.
- (3) FARREN, J.; DuPONT, J; NOECKER, F. Fabrication of a Carbon Steel-to-Stainless Steel Transition Joint Using Direct Laser Deposition - A Feasibility Study. **Welding Journal**, Bethlehem, v. 86, n. 3, p. 55-61, Mar. 2007.
- (4) ROBERTS, D, I.; RYDER, R. H.; VISWANATHAN, R. Performance of Dissimilar Welds in Service. **Journal of Pressure Vessel Technology**, Palo Alto, v. 107, n. 3, p. 247-254, Aug. 1985.
- (5) VENKATA RAMANA, P. et al. Microstructure and residual stress distribution of similar and dissimilar electron beam welds - Maraging steel to medium alloy medium carbon steel. **Materials and Design**, Hyderabad, v. 31, n. 2, p. 749-760, Aug. 2010.
- (6) LIPPOLD, J. C.; KOTECKI, D. J. **Welding Metallurgy and Weldability of Stainless Steels**. Hoboken: John Wiley & Sons, 2005. 357 p..
- (7) BAMFORD, W.; NEWTON, B.; SEEGER, D. Recent experience with weld overlay repair of indications in alloy 182 butt welds in two operating PWRs. In: PRESSURE VESSELS AND PIPING DIVISION CONFERENCE, 2006, Vancouver. **Proceedings...** Vancouver: ASME, 2006. p. 427-434.
- (8) EBERT, H. W. Nickel Alloy Filler Metal Review. **Welding Journal**, Madison, v. 83, n. 7, p. 170-173, 2004.
- (9) HICKLING, J. **Materials Reability Programa Crack Growth Rates for Evaluating Primary Water Stress Corrosion Cracking (PWSCC) of Alloy 82, 182, and 132 Welds (MRP-115)**. 6 ed. Palo Alto: EPRI, 2004. 186 p.
- (10) KIM, J. W. et al. Local mechanical properties of Alloy 82/182 dissimilar weld joint between SA508 Gr.1a and F316 SS at RT and 320 °C. **Journal of Nuclear Materials**, Dong-gu, v. 384, n. 3, p. 212–221, Feb. 2009.
- (11) ROBERGE, P. R. **Handbook of Corrosion Engineering**. New York: McGraw-Hill, 1999. 1128 p.
- (12) KOCH, G. H. Tests for stress-corrosion cracking. **Advanced Materials & Processes**, Dublin, v. 159, n. 8, p. 36-38, Aug. 2001.
- (13) SEDRIKS, J. A. **Stress Corrosion Cracking Test Methods**. Arlington: NACE, 1990. 87 p.
- (14) ASM - AMERICAN SOCIETY FOR METALS. **Corrosion of weldments**. ed 11. Ohio: Materials Park, 2007. 225 p.
- (15) KAPLAN, D; MURRY, G. **Metallurgy and Mechanics of Welding: Processes and Industrial Applications**. Chippenham: Jonh Wiley & Sons, 2008. p. 125
- (16) TSAI, W. T.; YU, C. L.; LEE, J. I. Effect of heat treatment on the sensitization of Alloy 182 weld. **Scripta Materialia**, Tainan, v. 53, n. 5, p. 505-509, Sep. 2005.
- (17) Gandy, D. **Carbon Steel Handbook**. Palo Alto: EPRI, 2007. 172 p.
- (18) MODENESI, P.; MARQUES, P; SANTOS, P. **Introdução à metalurgia da soldagem**. Belo Horizonte: Universidade Federal de Minas Gerais, 2016. 213 p.
- (19) OKUMURA, T.; TANIGUCHI, C. **Engenharia de Soldagem e Aplicações**. Rio de Janeiro: LTC - Livros Técnicos e Científicos, 1982. 493 p.

-
- (20) MCCAFFERTY, E. **Introduction to Corrosion Science**. New York: Springer New York, 2010. 575 p.
- (21) WOLYNEC, S. **Técnicas Eletroquímicas em Corrosão**. São Paulo: Edusp - Editora da Universidade de São Paulo, 2013. 163 p.
- (22) CAMPOS, W. R. C. et al. Effects of Post Weld Heat Treatment and Weld Overlay on the Residual Stress and Mechanical Properties in Dissimilar Metal Weld. In: INTERNATIONAL NUCLEAR ATLANTIC CONFERENCE, 2017, Belo Horizonte. **Proceedings...** Belo Horizonte: Associação Brasileira de Energia Nuclear, 2017, 13 p.
- (23) RIBEIRO, V. S. **Estudo de Técnicas de Redução de Tensão Residuais em Soldas Dissimilares Envolvendo Aço Carbono Ferrítico e Aço Inoxidável Austenítico com Adição das Ligas de Níquel 182/82**. 2017. 110 f. Dissertação (Mestrado) - Centro de Desenvolvimento de Tecnologia Nuclear, Belo Horizonte, 2017.
- (24) LU Y., et al. Effect of Welding Heat Input on the Corrosion Resistance of Carbon Steel Weld Metal, **Journal of Materials Engineering and Performance**, Tianjin, vol. 25, no. 2, p. 565–576, Feb. 2016.
- (25) DEEN, K. M. et al. Microstructural study and electrochemical behavior of low alloy steel weldment, **Materials and Design**, Lahore, vol. 31, no. 6, p. 3051–3055, Jun. 2010.
- (26) KUMARESH BABU, S. P.; NATARAJAN, S. Influence of heat input on high temperature weldment corrosion in submerged arc welded power plant carbon steel. **Materials and Design**, Tiruchirappalli, vol. 29, no. 5, p. 1036–1042, Apr. 2007.
- (27) MAKHDOOM, M. A. et al. Effect of multipasses on microstructure and electrochemical behavior of weldments, **Metallurgical and Materials Transactions A**, Lahore, vol. 44, no. 12, p. 5505–5512, Dec. 2013.
- (28) ALÉ, R.M.; JORGE, J. C. F.; REBELLO, J. M. A. Constituintes Microestruturais de Soldas de Aços C-Mn Baixa Liga. Parte II: Metal de Solda. **Soldagem & Materiais**. São Paulo, v. 5, n. 3, p.18-25. Fev. 1993
- (29) HER-HSIUNG HUANG ET AL. The influences of microstructure composition on the electrochemical of a516 steel weldment. **Corrosion Science**, CIDADE, v. 36, n. 6, p. 1027–1038, MES. 1994.
- (30) ALIZADEH, M.; BORDBAR, S. The influence of microstructure on the protective properties of the corrosion product layer generated on the welded API X70 steel in chloride solution. **Corrosion Science**, Kerman, v. 70, p. 170–179, May. 2013.
- (31) DAAVARI, M. et al. Mechanical and electrochemical behaviors of butt-welded high temperature steel pipes. **Engineering Failure Analysis**, Hafez Ave, v. 62, p. 287-299, Jan. 2016.